COBEM 2021 26th International Congress of Mechanical Engineering
November 22-26, 2021, Virtual Congress, Brazil

# COB-2021-2325
# On the Frequencies for Structural Health Monitoring in Plates with Symmetrical Damage: An Analytical Approach

**Kayc W. Lopes**
**Camila G. Gonsalez-Bueno**
Department of Mechanical Engineering, São Paulo State University (UNESP), School of Engineering of Ilha Solteira, Ilha Solteira, 15385-000, SP, Brazil
kayc.lopes@unesp.br, camila.gg.bueno@unesp.br

**Daniel J. Inman**
Department of Aerospace Engineering, University of Michigan, College of Engineering, Ann Arbor, MI 48109, United States of America
daninman@umich.edu

**Douglas D. Bueno**
Department of Mathematics, São Paulo State University (UNESP), School of Engineering of Ilha Solteira, Ilha Solteira, 15385-000, SP, Brazil
douglas.bueno@unesp.br

***Abstract.*** *Detecting incipient damage in structures is an important challenge for the engineering community. The design of structural health monitoring (SHM) systems usually involves selection of actuators and sensors, defining their positions on the structure and post-processing output signals. This article presents an approach to determine the optimal frequencies for damage detection in plates considering perpendicular incidence of longitudinal waves incoming in the damage. At these optimal frequencies are observed the maximum reflected and the minimum transmitted longitudinal wave amplitudes. Two damage detection indexes are introduced and if they are computed for the optimal frequencies it is possible to determine the damage depth. It is demonstrated that pulse-echo configuration is more convenient for damage detection because it involves higher wave amplitudes variation than the pitch-catch configuration. Numerical simulations are carried out by considering an aluminum plate, and the results show that the approach contributes to establish more efficient SHM systems.*

***Keywords:*** *Longitudinal Waves, Plates, Symmetrical Damage, Optimal Frequencies.*

## 1. INTRODUCTION

Engineers and researchers have employed important effort to develop new techniques for structural health monitoring (SHM). The development usually involves to detect incipient damage, which can contribute to reduce costs of maintenance and improve safety when using equipment (Baptista *et al.*, 2014; Lopes Júnior *et al.*, 2000; Gonsalez *et al.*, 2015).

Several approaches in the literature are focused on post-processing input and output signals obtained experimentally by using actuators and sensors placed on the structure (Hendrick, 1988; Dasgupta *et al.*, 2004; Ai *et al.*, 2018). They can also involve computational tools, as presented by Wu *et al.* (1992); Spillman *et al.* (1993); Doebling *et al.* (1996), and others.

SHM techniques based on post-processing input and output signals usually are demonstrated considering experimental data obtained from well-controlled tests conducted in laboratories. Authors have also considered more signals to include statistic-based procedures to infer a general efficiency of their methods. Although this a scientific method employed in engineering, SHM techniques have also been developed by investigating the wave propagation in the structure. Gonsalez-Bueno (2019) presents a strategy for monitoring beams with corrosion like-damage. The author considers longitudinal and flexural waves to demonstrate the wave interactions with symmetric and asymmetric damage. Optimum frequencies are defined to improve the damage detection. Piezoelectric transducers are employed to obtained experimental data to validate the accuracy of the proposed modeling.

Modeling wave propagation in structures allows one to investigate different issues in engineering, as shown by Szefi (2003); Nucera *et al.* (2015); Santos (2018), and others. Ahmida and Arruda (2002) obtain structural vibration modes from wave propagation using the Spectral Element Method (SEM). The authors introduce a parameter to measure the structural mode complexity. Mace (1984) investigates the vibration behavior of beams considering the effect of geometric disconti-

nuity. The article shows the importance of near-field waves for computing the amplitude of motion accurately. However, there is a few number of works in wave propagation focused on developing SHM techniques (Lee and Staszewski, 2003; Mal *et al.*, 2005; Ryue *et al.*, 2011; Gonsalez-Bueno, 2019).

The effects of geometric discontinuities on the coefficients of transmission and reflection waves are investigated by Younho Cho (2000); Schaal and Mal (2016) and Poddar and Giurgiutiu (2016) considering plate-like structures with cross-section changes. Thickness increasing and decreasing are employed to represent the discontinuity. On the other hand, different geometric shapes are considered by Cho and Rose (2000); Pau and Achillopoulou (2017); Kubrusly *et al.* (2019). Lowe and Diligent (2002) investigate the coefficient of reflection in a plate considering the presence of an asymmetrical rectangular crack in the case of incidence of S0 Lamb wave, the first symmetric lamb wave mode and characterized by the axial displacement of the middle plane of the plate. The authors show that resulting wave amplitudes exhibit periodic behavior according to the excitation frequency, with maximum and minimum magnitude depending on the damage width and excitation frequency. They highlight the importance of understanding this dynamic behavior for detecting the damage via non-destructive-based techniques considering the S0 lamb wave.

Based on this context, the present article introduces a modeling for the longitudinal wave propagation in a plate-like structure. It is considered a symmetric thickness reduction to represent the damage and a perpendicular incidence of longitudinal wave incoming in the damaged section. Transmitted and reflected wave amplitudes are obtained in relation to the incident wave amplitude and it is presented how they change over frequency. An analytical approach is employed by using the notation of state vector, which allows one to demonstrate that maximum wave amplitudes depend on the damage depth.

## 2. LONGITUDINAL WAVE PROPAGATION IN PLATES

The longitudinal displacements $u$ and $v$ respectively in the $x$ and $y$ directions (Fig. 1) in a rectangular plate are related by the following equation of motion (Giurgiutiu, 2014)

$$\begin{aligned}\frac{\partial^2 u}{\partial x^2}+\frac{(1-\nu_p)}{2}\frac{\partial^2 u}{\partial y^2}+\frac{(1+\nu_p)}{2}\frac{\partial^2 v}{\partial x\partial y}&=\frac{(1-\nu_p^2)\rho_p}{E_p}\frac{\partial^2 u}{\partial t^2}\\ \frac{\partial^2 v}{\partial y^2}+\frac{(1-\nu_p)}{2}\frac{\partial^2 v}{\partial x^2}+\frac{(1+\nu_p)}{2}\frac{\partial^2 u}{\partial x\partial y}&=\frac{(1-\nu_p^2)\rho_p}{E_p}\frac{\partial^2 v}{\partial t^2}\end{aligned} \tag{1}$$

where $E_p$ is the Young's modulus, $\rho_p$ is the material density and $\nu_p$ is the Poison's coefficient. The subscript $p$ indicates the undamaged plate. The solution of both equations in Eq. (1) is obtained by considering the vector $\mathbf{d}$ on the $x$-$y$ plane which contains the plate, such that $\mathbf{d}=u\vec{i}+v\vec{j}$, which allows one to rewrite the equation of motion as follows (Park *et al.*, 2001; Yeo *et al.*, 2017)

$$\frac{(1-\nu_p)}{2}\nabla^2\mathbf{d}+\frac{(1+\nu_p)}{2}\nabla\nabla\bullet\mathbf{d}=\frac{(1-\nu_p^2)\rho_p}{E_p}\frac{\partial^2\mathbf{d}}{\partial t^2} \tag{2}$$

where $\vec{\mathbf{i}}$ and $\vec{\mathbf{j}}$ are unitary vectors in the $x$ and $y$ directions, respectively, $\bullet$ indicates the scalar product, $\nabla=\frac{\partial()\mathbf{i}}{\partial x}+\frac{\partial()\mathbf{j}}{\partial y}$ is the gradient operator and $\nabla^2=\nabla\bullet\nabla$ is the Laplacian.

The solution vector $\mathbf{d}$ can be conveniently given by considering potential functions $\varphi(x,y,t)$ and $\psi(x,y,t)$, such that (Miklowitz, 1978)

$$\mathbf{d}(x,y,t)=\nabla\varphi(x,y,t)+\nabla\times\boldsymbol{\psi}(x,y,t) \tag{3}$$

where $\varphi(x,y,t)$ is a scalar function representing the potential linear displacement and $\psi(x,y,t)$ represents the potential angular displacement and normal to the plate plane, i.e., $\nabla\bullet\psi=0$ (Park *et al.*, 2001). Substituting Eq. (3) into (2), it is obtained (see appendix A for details):

$$\nabla\left(\nabla^2\varphi-\frac{(1-\nu_p^2)\rho_p}{E_p}\frac{\partial^2\varphi}{\partial t^2}\right)+\nabla\times\left(\frac{(1-\nu_p)}{2}\nabla^2\boldsymbol{\psi}-\frac{(1-\nu_p^2)\rho_p}{E_p}\frac{\partial^2\boldsymbol{\psi}}{\partial t^2}\right)=0 \tag{4}$$

Equation (4) allows one to write $\nabla^2\varphi=\dfrac{1}{c_l^2}\dfrac{\partial^2\varphi}{\partial t^2}$ and $\nabla^2\psi=\dfrac{1}{c_s^2}\dfrac{\partial^2\boldsymbol{\psi}}{\partial t^2}$, which are respectively related to the longitudinal and the shear waves in the middle plane of the plate. Their respective phase velocities are $c_l=\sqrt{E_p/[\rho_p(1-\nu_p^2)]}$

and $c_s = \sqrt{G_p/\rho_p}$, where $G_p$ is the shear modulus. The shear waves can be neglected, which allows one to introduce the following equation to compute the potential linear displacement (Park *et al.*, 2001)

$$\varphi(x, y, \omega) = [B_1 e^{i(-k_1 x - k_2 y)} + B_2 e^{i(k_1 x - k_2 y)} + B_3 e^{i(k_1 x + k_2 y)} + B_4 e^{i(-k_1 x + k_2 y)}] e^{-i\omega t} \tag{5}$$

where $B_1$ to $B_4$ are potential function amplitudes, $k_1$ and $k_2$ are component of the longitudinal wavenumber respectively in the $x$ and $y$ directions, $i^2 = -1$ and $\omega$ is the circular frequency. Considering the case of wave propagation only in the $x$ direction, it is possible to write that $k_1 = k$ and $k_2 = 0$, where $k = \omega/c_l$ is the wavenumber. $k \equiv k_p$ for the plate undamaged region and $k_d$ for the damaged one.

Based on Eq. (5) and considering that $u = \partial\varphi/\partial x$ e $v = \partial\varphi/\partial y$ (Park *et al.*, 2001), the longitudinal displacements are given by

$$\begin{aligned} u(x, y, \omega) &= [A_r e^{-ikx} - A_l e^{+ikx}] e^{-i\omega t} \\ v(x, y, \omega) &= 0 \end{aligned} \tag{6}$$

The wave amplitudes are $A_r = -(B_1 + B_4)ik$ and $A_l = -(B_2 + B_3)ik$, where subscripts $r$ (*right*) and $l$ (*left*) indicate positive and negative directions of $x$ axis, respectively, as illustrated in Fig. 1.

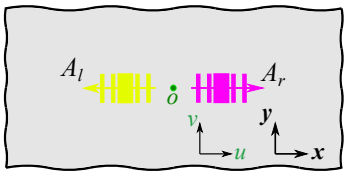


Figure 1. Longitudinal waves propagating from a point $o$ on the plate, where $A_{(.)}$ is the wave amplitude and the subscripts $r$ and $l$ indicate respectively right and left. Point $o$ indicates the coordinate system origin. $u$ and $v$ are the displacements in the $x$ and $y$ directions, respectively.

The line forces per unit of displacement in the $x$ and $y$ directions are $N_x$ and $N_y$, respectively given by (Giurgiutiu, 2014; Radwańska *et al.*, 2017)

$$\begin{aligned} N_x &= \frac{E_p h_p}{1 - \nu_p^2} \left( \frac{\partial u}{\partial x} + \nu_p \frac{\partial v}{\partial y} \right) \\ N_y &= \frac{E_p h_p}{1 - \nu_p^2} \left( \nu_p \frac{\partial u}{\partial x} + \frac{\partial v}{\partial y} \right) \end{aligned} \tag{7}$$

where $h_p$ is the plate thickness. Substituting Eq. (6) into Eq. (7), it is possible to write

$$\begin{aligned} N_x &= \frac{E_p h_p}{1 - \nu_p^2} \left[ -A_r ike^{-ikx} - A_l ike^{+ikx} \right] e^{-i\omega t} \\ N_y &= \frac{E_p h_p}{1 - \nu_p^2} \left[ -A_r ik\nu e^{-ikx} - A_l ik\nu e^{+ikx} \right] e^{-i\omega t} \end{aligned} \tag{8}$$

From Eqs. (6) and (8), the state vector $\mathbf{h} = \{u \quad N_x\}^T$ is defined. In this case, $N_y$ is proportional to $N_x$ ($N_y = \nu N_x$), them just one them is used. Brennan (1994) noted that is convenient to introduce the transformation matrix $\mathbf{H}$, the spatial transformation matrix $\mathbf{T}$ and the vector of wave amplitudes $\mathbf{a}$ to rewrite a state-vector-based notation such that

$$\mathbf{h}(x, \omega) = \mathbf{H}(\omega)\mathbf{T}(x, \omega)\mathbf{a}(\omega) \tag{9}$$

Note that the dependency of $x$ and $\omega$ indicated in Eq. (9) is omitted in this article by simplicity. As made by Brennan (1994) for the case of beam-like structures, the equations for the plate considered herein can be similarly rearranged, and the following matrices and vector can be defined

$$\mathbf{H} = \begin{bmatrix} 1 & -1 \\ \dfrac{-E_p h_p ik}{(1 - \nu_p^2)} & \dfrac{-E_p h_p ik}{(1 - \nu_p^2)} \end{bmatrix} \tag{10}$$

$$\mathbf{T} = diag \left( \begin{array}{cc} e^{-ikx}, e^{ikx} \end{array} \right) \tag{11}$$

$$\mathbf{a} = \left\{ \begin{array}{cc} A_r & A_l \end{array} \right\}^T \tag{12}$$

where $diag(\ )$ indicates a diagonal matrix.

### 2.1 Longitudinal Wave Propagation in thin Plates with Symmetrical Damage

Shen and Pierre (1990) introduce that a symmetric damage can be represented through a local thickness reduction. In particular to the plate, it is considered a damage with width $l_x << L_x$ and length $L_y$, where $L_x$ and $L_y$ are the lengths of the plate in the $x$ and $y$ directions, respectively. Based on this configuration, the following section introduces the relation between wave amplitudes (i.e., transmitted or reflected in relation to the incident waves). It is assumed that an actuator $C$ is placed on the left-hand side of the damage. A sensor $S_r$ is considered on the right-hand side of the damage. Using the state-vector-based notation previously introduced in the present article, it is investigated a configuration corresponding to the actuator generating waves in the positive direction of $x$.

#### 2.1.1 Incident Wave Propagating in the positive direction of $x$

Figure 2 shows an infinite plate with an actuator $C$ placed on the point $p$ and a sensor $S_r$ placed on the point $a$. It is assumed that the transducer in $C$ works as actuator and sensor. Assuming that longitudinal waves are generated in a positive direction of $x$, a transmitted longitudinal wave is obtained by $S_r$ from the point $s$, whereas a reflected wave is obtained by $C$ from the point $q$, as illustrated in Fig. 2.

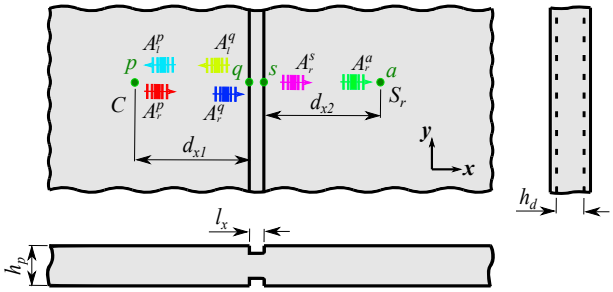


Figure 2. Symmetric damage with width $l_x$ in the $x$ direction and $L_y$ length in the $y$ direction. Actuator $C$ excites the plate in the positive direction of $x$. Sensor $S_r$ measures the transmitted wave and sensor $C$ measures the reflected wave. Damage depth equal to $(h_p - h_d)/2$.

Considering the force and displacement continuity at the point $q$, $\mathbf{h}_l^q = \mathbf{h}_r^q$ and, hence, $\mathbf{H}_{(p)}\mathbf{a}_{(l)}^q = \mathbf{H}_{(d)}\mathbf{a}_{(r)}^q$, where the subscripts $p$ and $d$ indicate the plate (undamaged region) and damage regions, respectively. Based on Eq. (12), $\mathbf{a}_{(l)}^q = \{A_r^{q(i)} \quad A_l^{q(o)}\}^T$, where the superscripts $i$ and $o$ indicate respectively the incoming and the outgoing waves at the point $q$. Similarly, $\mathbf{H}_{(d)}\mathbf{a}_{(l)}^s = \mathbf{H}_{(p)}\mathbf{a}_{(r)}^s$, where $\mathbf{a}_{(l)}^s = \mathbf{T}_{(d)}\mathbf{a}_{(r)}^q$ and $\mathbf{T}_{(d)}$ is obtained from Eq. (11) for $x = l_x$. Note that $\mathbf{a}_{(r)}^s = \{0 \quad A_r^{s(o)}\}^T$ because no wave comes to the point $s$ from the right-hand side of the plate. To establish a relation between $\mathbf{a}_{(l)}^q$ and $\mathbf{a}_{(r)}^s$, the following equation can be introduced $\mathbf{H}_{(d)}\mathbf{T}_{(d)}[\mathbf{H}_{(d)}]^{-1}\mathbf{H}_{(p)}\mathbf{a}_{(l)}^q - \mathbf{H}_{(p)}\mathbf{a}_{(r)}^s = \mathbf{0}$ (see appendix A 1 for details). Rearranging this last equation, it is possible to demonstrate the following equation:

$$\frac{A_r^{s(o)}}{A_r^{q(i)}} = \frac{4QF}{F^2\left(1+Q\right)^2 - \left(1-Q\right)^2} \tag{13}$$

$$\frac{A_l^{q(o)}}{A_r^{q(i)}} = \frac{\left(Q^2-1\right)\left(F^2-1\right)}{F^2\left(1+Q\right)^2 - \left(1-Q\right)^2} \tag{14}$$

where $Q = Hh$. The exponential-based function $F$ is $F = e^{ik_d l_x}$. In addition, $h = h_d/h_p$ and $H = \sqrt{E\rho}$, where $E = E_d/E_p$, $\rho = \rho_d/\rho_b$. It is assumed $\nu_p = \nu_d$.

The spatial transformation matrix $\mathbf{T}$ can properly be employed to rewrite $A_r^{s(o)}$ at the point $a$ (sensor $S_r$) and, similarly, $A_l^{q(o)}$ at the point $p$ (sensor $C$) - note that $A_r^{q(i)} = A_r^p e^{-ik_p d_{x1}}$, $A_l^p = A_l^{q(o)} e^{+ik_p(-d_{x1})}$ and $A_r^a = A_r^{s(o)} e^{-ik_p d_{x2}}$, where $A_r^p$ is the wave amplitude generated by the actuator ($C$), $A_r^a$ is the transmitted and $A_l^p$ is the reflected longitudinal waves, which are described by the following equations

$$\frac{A_r^a}{A_r^p} = \frac{4QFe^{-ik_p\phi}}{F^2\left(1+Q\right)^2 - \left(1-Q\right)^2} \tag{15}$$

$$\frac{A_l^p}{A_r^p} = \frac{\left(Q^2-1\right)\left(F^2-1\right)e^{-ik_p\gamma}}{F^2\left(1+Q\right)^2 - \left(1-Q\right)^2} \tag{16}$$

where $\phi = (d_{x1} + d_{x2})$ and $\gamma = 2d_{x1}$.

## 3. RESULTS AND DISCUSSION

This section presents numerical simulations to demonstrate the approach proposed to investigate the interactions between damage and waves in a thin plate. It is considered an aluminum plate with $\rho_p = 2710$ kg/m$^3$, $E_p = 68$ GPa, $\nu_p = 0.31$, $d_{x1} = d_{x2} = 0.15$ m, $h_p = 0.0015$ m m and $l_x = 0.01$ m.

The actuator $C$ works as sensor and capture the reflected longitudinal waves and sensor $S_r$ is horizontally aligned with the actuator (i.e., points $a$ and $p$ on a same horizontal line). For this particular case, Fig. 3 shows that the transmitted wave amplitude is equal to the incident wave for the frequencies corresponding to $\frac{l_x}{\lambda_d} = (n+1)/2$, with $n = 0,\ 1, ...$, where $\lambda_d = \lambda_p$, i.e, the wavelength of the plate - assuming damaged and undamaged regions with the same physical properties. It is possible to note that at these frequencies the transmitted wave does not detect the damage. Similar results are observed for the reflected waves at these frequencies, as shown in Fig. 3. On the other hand, at frequencies corresponding to $\frac{l_x}{\lambda_d} = (n+1)/4$, with $n = 0,\ 2,\ 4, ...$, it is noted an important variation in both transmitted and reflected wave amplitudes, which means that $f_t = f_r \equiv f_0 = \left(\frac{n+1}{4l_x}\right)\sqrt{E_p/[\rho_p(1-\nu_p^2)]}$ Hz, for $n = 0, 2, 4, 6, ...$, are respectively the optimal frequencies for damage detection using the pitch-catch (transmitted wave) and the pulse-echo (reflected wave) configurations, whatever the depth of the damage $(h_p - h_d)/2$. Gonsalez-Bueno (2019) showed similar results for beam-like structures, including comparisons between these two SHM configurations.

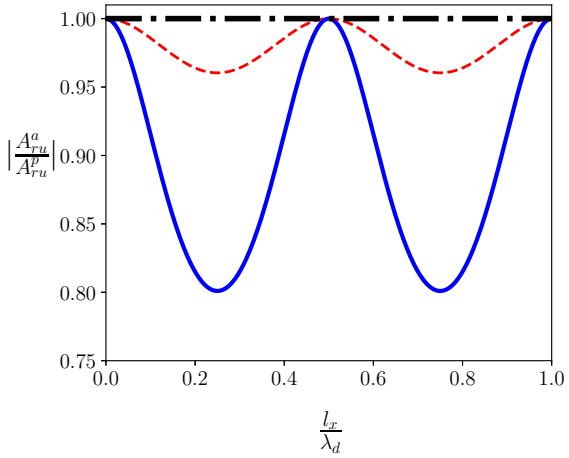


Figure 3. Magnitude of transmitted wave amplitude in relation to the incident wave $(|A^a_r/A^p_r|)$ in terms of $l_x/\lambda_d$ for different damage depth: $h = 1$ (i.e., undamaged plate, dash-dotted line), $h = 0.75$ (dashed line) and $h = 0.5$ (continuous line).

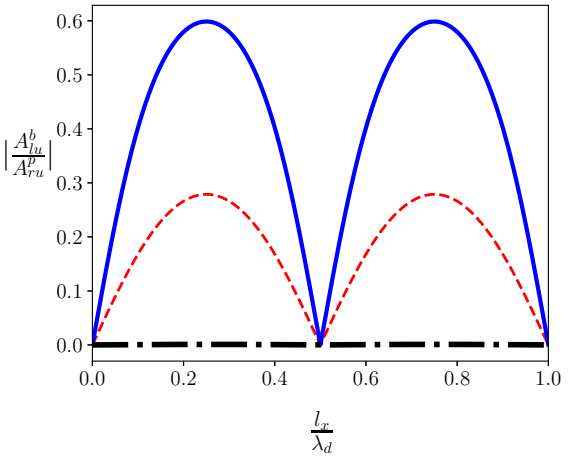


Figure 4. Magnitude of reflected wave amplitude in relation to the incident wave $(|A^p_l/A^p_r|)$ in terms of $l_x/\lambda_d$ for different damage depth: $h = 1$ for (i.e., undamaged plate, dash-dotted line), $h = 0.75$ (dashed line) and $h = 0.5$ (continuous line).

Because the maximum reflected $A_r|_{max}$ and the minimum transmitted $A_t|_{min}$ waves amplitudes are only dependent

on the ratio $h$, it is possible to write $\frac{A_r}{A_i}\Big|_{max} = \frac{1-h^2}{1+h^2}$ and $\frac{A_t}{A_i}\Big|_{min} = \frac{2h}{1+h^2}$, which occurs at the optimal frequencies. These results show that $\frac{A_r}{A_i}\Big|_{max} = \frac{A_t}{A_i}\Big|_{min} = 1/\sqrt{2}$ when $h = (\sqrt{2}-1) \approx 0.4142$, i.e., $h_d \approx 0.4142 h_p$, as shown in Fig. 5, which corresponds to damage depth equal to $d/2 \equiv d_c \approx 29.29\%$ of the plate thickness (symmetrically on its top and bottom surfaces).

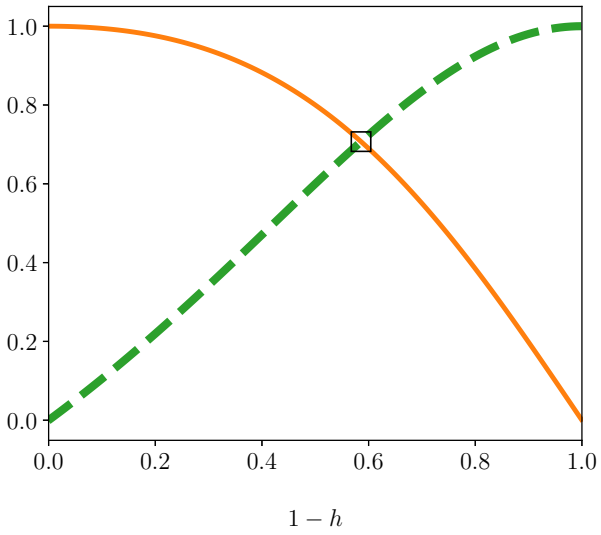


Figure 5. Maximum reflected wave amplitude $\frac{A_r}{A_i}\Big|_{max}$ (continuous line) and minimum transmitted wave amplitude $\frac{A_t}{A_i}\Big|_{min}$ (dashed line) in terms of $h$. These amplitudes are equal each other for a damage depth $29.29\%$ of the plate thickness, symmetrically on its top and bottom surfaces (□ symbol).

The index $I_t = (A_i - A_t|_{min})/A_i$ can be used to detect the damage at the optimal frequency using the transmitted wave. It is rewritten by $I_t = (1-h)^2/(1+h^2)$, such that $I_t = 0$ for the healthy structure. Similarly, $I_r = (A_r|_{max})/A_i = (1-h^2)/(1+h^2)$ can be applied to detect the damage using the reflected wave. To compare pulse-echo and pitch-catch configurations, it is possible to evaluate when $I_r > I_t$. This inequality implies $h < 1$, which means that, whatever the depth of damage, the pulse-echo configuration (i.e., the reflected wave) provides wave amplitudes higher than the pitch-catch, and because of this it is more convenient to detect the damage.

## 4. FINAL REMARKS

The present article introduced an approach to evaluate longitudinal waves focused on structural health monitoring in plates with symmetric damage. It was shown that there are optimal frequencies to observe the interaction between damage and transmitted and reflected longitudinal waves. The SHM analyst can previously define the damage width $l_x$ to be detected, which allows one to compute an optimal frequency. At these optimal frequencies, transmitted and reflected wave amplitudes are obtained proportional to the coefficients $\frac{2h}{1+h^2}$ and $\frac{1-h^2}{1+h^2}$, respectively. These wave amplitudes can be determined using these coefficients multiplied by the wave amplitude generated by the actuator because the magnitude of this last one is equal to the incident wave incoming to the damage (there is only a phase between them).

For the case of perpendicular incidence of longitudinal waves on the damage, the optimal frequencies for damage detection using SHM systems are obtained when the relation $\frac{l_x}{\lambda_d} = (n+1)/4$ is well established, being the optimal frequencies equal to $f_0 = \left(\frac{n+1}{4l_x}\right)\sqrt{E_p/[\rho_p(1-\nu_p^2)]}$ Hz. However, it changes when there is a variation in the incidence angle and this equation can be used just for the case shown in this article. The change in the optimal frequency occurs because the reflected and transmitted waves will be collected in different points of the plate, so the methodology has to be adapted.

Damage detection indexes are defined in terms of the maximum reflected and minimum transmitted wave amplitudes. They demonstrated that pulse-echo configuration is more convenient for damage detection because it involves higher wave amplitudes than the pitch-catch configuration, which is an advantage to carry out the measurements in practical applications. These damage detection indexes ($I_t$ and $I_r$) can be employed to identify the damage depth computing $h_c = \frac{I}{1+I} h_p$, where $I = I_t/I_r$.

## 5. ACKNOWLEDGEMENTS

The first and last authors thank to the São Paulo Research Foundation (FAPESP), grant number 2019/21149-9, and Brazilian National Council for Scientific and Technological Development (CNPq), grant number 133397/2019-0, for funding this research.

## 6. REFERENCES

Ahmida, K. and Arruda, J., 2002. "On the relation between complex modes and wave propagation phenomena". *Journal of Sound and Vibration*, Vol. 255, No. 4, pp. 663 – 684. ISSN 0022-460X. doi:https://doi.org/10.1006/jsvi.2001.4183. URL http://www.sciencedirect.com/science/article/pii/S0022460X01941835.

Ai, D., Luo, H., Wang, C. and Zhu, H., 2018. "Monitoring of the load-induced rc beam structural tension/compression stress and damage using piezoelectric transducers". *Engineering Structures*, Vol. 154, pp. 38 – 51. ISSN 0141-0296. doi:https://doi.org/10.1016/j.engstruct.2017.10.046. URL http://www.sciencedirect.com/science/article/pii/S0141029617321624.

Baptista, F.G., Budoya, D.E., Almeida, V.A.D.d. and Ulson, J.A.C., 2014. "An experimental study on the effect of temperature on piezoelectric sensors for impedance-based structural health monitoring". *Sensors*, Vol. 14, No. 1, pp. 1208–1227. ISSN 1424-8220. doi:10.3390/s140101208. URL http://www.mdpi.com/1424-8220/14/1/1208.

Brennan, M.J., 1994. *Active Control of Waves on one-dimensional Structures*. Ph.D. thesis, University of Southampton. URL https://eprints.soton.ac.uk/69563/.

Cho, Y. and Rose, J.L., 2000. "An elastodynamic hybrid boundary element study for elastic guided wave interactions with a surface breaking defect". *International Journal of Solids and Structures*, Vol. 37, No. 30, pp. 4103 – 4124. ISSN 0020-7683. doi:https://doi.org/10.1016/S0020-7683(99)00142-0. URL http://www.sciencedirect.com/science/article/pii/S0020768399001420.

Dasgupta, D., KrishnaKumar, K., Wong, D. and Berry, M., 2004. "Negative selection algorithm for aircraft fault detection". In G. Nicosia, V. Cutello, P.J. Bentley and J. Timmis, eds., *Artificial Immune Systems*. Springer Berlin Heidelberg, Berlin, Heidelberg, pp. 1–13. ISBN 978-3-540-30220-9.

Doebling, S., Farrar, C., Prime, M. and Shevitz, D., 1996. "Damage identification and health monitoring of structural and mechanical systems from changes in their vibration characteristics: A literature review". *Technical Report No. LA-13070-MS*, Vol. 30. doi:10.2172/249299.

Giurgiutiu, V., 2014. "Chapter 4 - vibration of plates". In V. Giurgiutiu, ed., *Structural Health Monitoring with Piezoelectric Wafer Active Sensors (Second Edition)*, Academic Press, Oxford, pp. 145 – 197. Second edition edition. ISBN 978-0-12-418691-0. doi:https://doi.org/10.1016/B978-0-12-418691-0.00004-6. URL http://www.sciencedirect.com/science/article/pii/B9780124186910000046.

Gonsalez, C.G., Silva, S., Brennan, M.J. and Lopes Junior, V., 2015. "Structural damage detection in an aeronautical panel using analysis of variance". *Mechanical Systems and Signal Processing*, Vol. 52-53, pp. 206 – 216. ISSN 0888-3270. doi:https://doi.org/10.1016/j.ymssp.2014.04.015. URL http://www.sciencedirect.com/science/article/pii/S0888327014001216.

Gonsalez-Bueno, C.G., 2019. "An investigation into the way in which longitudinal and flexural waves interact with corrosion-like damage". URL http://hdl.handle.net/11449/181311. Ph.D Thesis, São Paulo State University (UNESP), School of Engineering of Ilha Solteira, Department of Mechanical Engineering, SP, Brazil.

Hendrick, S., 1988. *Damage detection and location in large space trusses*. doi:10.2514/6.1988-2461. URL https://arc.aiaa.org/doi/abs/10.2514/6.1988-2461.

Kubrusly, A.C., von der Weid, J.P. and Dixon, S., 2019. "Experimental and numerical investigation of the interaction of the first four sh guided wave modes with symmetric and non-symmetric discontinuities in plates". *NDT & E International*, Vol. 108, p. 102175. ISSN 0963-8695. doi:https://doi.org/10.1016/j.ndteint.2019.102175. URL http://www.sciencedirect.com/science/article/pii/S0963869519303500.

Lee, B.C. and Staszewski, W.J., 2003. "Modelling of lamb waves for damage detection in metallic structures: Part ii. wave interactions with damage". *Smart Materials and Structures*, Vol. 12, No. 5, p. 815. URL http://stacks.iop.org/0964-1726/12/i=5/a=019.

Lopes Júnior, V., Park, G., Cudney, H.H. and Inman, D.J., 2000. "Impedance-based structural health monitoring with artificial neural networks". *Journal of Intelligent Material Systems and Structures*, Vol. 11, No. 3, pp. 206–214. doi:10.1106/H0EV-7PWM-QYHW-E7VF. URL https://doi.org/10.1106/H0EV-7PWM-QYHW-E7VF.

Lowe, M.J.S. and Diligent, O., 2002. "Low-frequency reflection characteristics of the s0 lamb wave from a rectangular notch in a plate". *The Journal of the Acoustical Society of America*, Vol. 111, No. 1, pp. 64–74. doi:10.1121/1.1424866. URL https://doi.org/10.1121/1.1424866.

Mace, B., 1984. "Wave reflection and transmission in beams". *Journal of Sound and Vibration*, Vol. 97, No. 2, pp. 237 – 246. ISSN 0022-460X. doi:https://doi.org/10.1016/0022-460X(84)90320-1. URL http://www.sciencedirect.com/science/article/pii/0022460X84903201.

Mal, A., Ricci, F., Banerjee, S. and Shih, F., 2005. "A conceptual structural health monitoring system based on vibration and wave propagation". *Structural Health Monitoring*, Vol. 4, No. 3, pp. 283–293. doi:10.1177/1475921705055254. URL https://doi.org/10.1177/1475921705055254.

Miklowitz, J., 1978. *The Theory of Elastic Waves and Waveguides*. Applied mathematics and mechanics. North Holland Publishing Company. ISBN 9780720405514. URL https://books.google.com.br/books?id=YiAbAQAAIAAJ.

Nucera, C., White, S., Chen, Z.M., Kim, H. and di Scalea, F.L., 2015. "Impact monitoring in stiffened composite aerospace panels by wave propagation". *Structural Health Monitoring*, Vol. 14, No. 6, pp. 547–557. doi:10.1177/1475921715599600. URL https://doi.org/10.1177/1475921715599600.

Park, D.H., Hong, S.Y., Kil, H.G. and Jeon, J.J., 2001. "Power flow models and analysis of in-plane waves in finite coupled thin plates". *Journal of Sound and Vibration*, Vol. 244, No. 4, pp. 651 – 668. ISSN 0022-460X. doi:https://doi.org/10.1006/jsvi.2000.3517. URL http://www.sciencedirect.com/science/article/pii/S0022460X0093517X.

Pau, A. and Achillopoulou, D., 2017. "Interaction of shear and rayleigh–lamb waves with notches and voids in plate waveguides". *Materials*, Vol. 10, p. 841. doi:10.3390/ma10070841.

Poddar, B. and Giurgiutiu, V., 2016. "Scattering of lamb waves from a discontinuity: An improved analytical approach". *Wave Motion*, Vol. 65, pp. 79 – 91. ISSN 0165-2125. doi:https://doi.org/10.1016/j.wavemoti.2016.03.009. URL http://www.sciencedirect.com/science/article/pii/S0165212516300051.

Radwańska, M., Stankiewicz, A., Wosatko, A. and Pamin, J., 2017. *Plate and Shell Structures: Selected Analytical and Finite Element Solutions*. Wiley. ISBN 9781118934548. URL https://books.google.com.br/books?id=hdWdDQAAQBAJ.

Ryue, J., Thompson, D., White, P. and Thompson, D., 2011. "Wave reflection and transmission due to defects in infinite structural waveguides at high frequencies". *Journal of Sound and Vibration*, Vol. 330, No. 8, pp. 1737 – 1753. ISSN 0022-460X. doi:https://doi.org/10.1016/j.jsv.2010.10.034. URL http://www.sciencedirect.com/science/article/pii/S0022460X10007200.

Santos, R.B., 2018. *An alternative approach to design periodic rods*. Ph.D. thesis. URL http://hdl.handle.net/11449/153135. Ph.D Thesis, São Paulo State University (UNESP), School of Engineering of Ilha Solteira, Department of Mechanical Engineering, SP, Brazil.

Schaal, C. and Mal, A., 2016. "Lamb wave propagation in a plate with step discontinuities". *Wave Motion*, Vol. 66, pp. 177 – 189. ISSN 0165-2125. doi:https://doi.org/10.1016/j.wavemoti.2016.06.012. URL http://www.sciencedirect.com/science/article/pii/S0165212516300671.

Shen, M.H.H. and Pierre, C., 1990. "Natural modes of Bernoulli-Euler beams with symmetric cracks". *Journal of Sound and Vibration*, Vol. 138, No. 1, pp. 115–134.

Spillman, W., Huston, D., Fuhr, P. and Lord, J., 1993. "Neural network damage detection in a bridge element". *Proceedings of SPIE - The International Society for Optical Engineering*. doi:10.1117/12.147985.

Szefi, J.T., 2003. *Helicopter gearbox isolation using periodically layered fluidic isolators*. Ph.D. thesis, The Pennsylvania State University.

Wu, X., Ghaboussi, J. and Garrett, J., 1992. "Use of neural networks in detection of structural damage". *Computers & Structures*, Vol. 42, No. 4, pp. 649 – 659. ISSN 0045-7949. doi:https://doi.org/10.1016/0045-7949(92)90132-J. URL http://www.sciencedirect.com/science/article/pii/004579499290132J.

Yeo, S.J., Hong, S.Y., Song, J.H. and Kwon, H.W., 2017. "Vibrational energy flow models for dilatational wave in elastic solids". *Advances in Mechanical Engineering*, Vol. 9, No. 12, p. 1687814017740709. doi:10.1177/1687814017740709. URL https://doi.org/10.1177/1687814017740709.

Younho Cho, 2000. "Estimation of ultrasonic guided wave mode conversion in a plate with thickness variation". *IEEE Transactions on Ultrasonics, Ferroelectrics, and Frequency Control*, Vol. 47, No. 3, pp. 591–603. ISSN 1525-8955. doi:10.1109/58.842046.

## 7. RESPONSIBILITY NOTICE

The authors are solely responsible for the printed material included in this paper.

## A Equation of Motion

This appendix presents algebraic rearrangements to obtain the equation of motion (Eq. 20). Complementary information can be found in Park *et al.* (2001). The first step is to substitute Eq. (3) into (2), such that

$$\frac{(1-\nu)}{2}\nabla^2\left[\nabla\varphi+\nabla\times\boldsymbol{\psi}\right]+\frac{(1+\nu)}{2}\nabla(\nabla\bullet\left[\nabla\varphi+\nabla\times\boldsymbol{\psi}\right])=\frac{(1-\nu^2)\rho}{E}\frac{\partial^2}{\partial t^2}\left[\nabla\varphi+\nabla\times\boldsymbol{\psi}\right] \tag{17}$$

where $\nabla\bullet\nabla\varphi=\nabla^2\varphi$ and $\nabla\bullet(\nabla\times\psi)=0$ (Park *et al.*, 2001), which allows one to rewrite

$$\frac{(1-\nu)}{2}\nabla^2\left[\nabla\varphi+\nabla\times\boldsymbol{\psi}\right]+\frac{(1+\nu)}{2}\nabla(\nabla^2\varphi)=\frac{(1-\nu^2)\rho}{E}\frac{\partial^2}{\partial t^2}\left[\nabla\varphi+\nabla\times\boldsymbol{\psi}\right] \tag{18}$$

considering that $\nabla^2(\nabla\varphi) = \nabla(\nabla^2\varphi)$ and $\nabla^2(\nabla\times\psi) = \nabla\times(\nabla^2\psi)$. In this case, it is possible to obtain $\frac{\partial^2}{\partial t^2}(\nabla\times\psi) = \nabla\times(\frac{\partial^2}{\partial t^2}\psi)$ and $\frac{\partial^2}{\partial t^2}(\nabla\varphi) = \nabla(\frac{\partial^2}{\partial t^2}\varphi)$, which allows one to write Eq. (18) in the following form

$$\frac{(1-\nu)}{2}\left[\nabla(\nabla^2\varphi) + \nabla\times(\nabla^2\boldsymbol{\psi})\right] + \frac{(1+\nu)}{2}\nabla(\nabla^2\varphi) = \frac{(1-\nu^2)\rho}{E}\left[\nabla\left(\frac{\partial^2\varphi}{\partial t^2}\right) + \nabla\times\left(\frac{\partial^2\boldsymbol{\psi}}{\partial t^2}\right)\right] \tag{19}$$

From this last equation, it is possible to obtain

$$\nabla\left(\nabla^2\varphi - \frac{(1-\nu^2)\rho}{E}\frac{\partial^2\varphi}{\partial t^2}\right) + \nabla\times\left(\frac{(1-\nu)}{2}\nabla^2\boldsymbol{\psi} - \frac{(1-\nu^2)\rho}{E}\frac{\partial^2\boldsymbol{\psi}}{\partial t^2}\right) = 0 \tag{20}$$

## A 1 Incoming and Outgoing Waves Vectors

The state vector at the point $q$ shown in Fig. 2 is $\mathbf{h}_l^q = \mathbf{H}_{(p)}\mathbf{a}_{(l)}^q$ for the left-hand side and $\mathbf{h}_d^q = \mathbf{H}_{(d)}\mathbf{a}_{(r)}^q$ for the damaged side. It allows one to obtain $\mathbf{a}_{(r)}^q = [\mathbf{H}_{(d)}]^{-1}\mathbf{H}_{(p)}\mathbf{a}_{(l)}^q$, where $\mathbf{a}_{(l)}^q = \{A_r^{q(i)}\ \ A_l^{q(o)}\}^T$. Points $q$ and $s$ are related by $\mathbf{a}_{(l)}^s = \mathbf{T}_{(d)}\mathbf{a}_{(r)}^q$, where $\mathbf{T}_{I(d)}$ is determined by Eq. (11) considering $k \equiv k_d$ and $x \equiv l_x$ for geometric properties of the damage. Using these equations it is possible to write $\mathbf{a}_{(l)}^s = \mathbf{T}_{(d)}[\mathbf{H}_{(d)}]^{-1}\mathbf{H}_{(p)}\mathbf{a}_{(l)}^q$. Similarly, at the point $s$ $\mathbf{H}_{(d)}\mathbf{a}_{(l)}^s = \mathbf{H}_{(p)}\mathbf{a}_{(r)}^s$ because $\mathbf{h}_l^s = \mathbf{h}_r^s$, where $\mathbf{a}_{(r)}^s = \{A_r^{s(o)}\ \ 0\}^T$. Then,

$$\mathbf{H}_{(d)}\mathbf{T}_{(d)}[\mathbf{H}_{(d)}]^{-1}\mathbf{H}_{(p)}\mathbf{a}_{(l)}^q - \mathbf{H}_{(p)}\mathbf{a}_{(r)}^s = \mathbf{0} \tag{21}$$

Equation (21) can be rearranged to write $\mathbf{a}_{out} = \mathbf{C}^{-1}\mathbf{B}\mathbf{a}_{in}$, where $\mathbf{a}_{out}$ is the vector of wave amplitudes resulting from the interaction between incident wave and damage. It corresponds to the outgoing waves such that $\mathbf{a}_{out} = \{A_r^{s(o)}\ \ A_l^{q(o)}\}^T$. On the other hand, vector with incoming waves is $\mathbf{a}_{in} = \{A_r^{q(i)}\ 0\}^T$. The matrices $\mathbf{B}$ and $\mathbf{C}$ are given by

$$\mathbf{B} = \left[\left(-\mathbf{H}_{(d)}\mathbf{T}_{(d)}[\mathbf{H}_{(d)}]^{-1}\mathbf{H}_{(p)}\right)_1 \quad \left(\mathbf{H}_{(p)}\right)_2\right] \tag{22}$$

$$\mathbf{C} = \left[\left(-\mathbf{H}_{(p)}\right)_1 \quad \left(\mathbf{H}_{(d)}\mathbf{T}_{(d)}[\mathbf{H}_{(d)}]^{-1}\mathbf{H}_{(p)}\right)_2\right] \tag{23}$$

where $(\ )_1$ and $(\ )_2$ denote respectively first and second columns of the matrices inside the round brackets.